

# CONTACT LENSES DETECTION USING LOCAL PHASE QUANTIZATION AND BINARY GABOR PATTERN

*A Thesis Submitted  
in Partial Fulfillment of the Requirements  
for the Degree of  
Bachelor - Master of Technology*

*by*

**Lovish**

**Y9227309**

*under the guidance of  
Prof. Phalguni Gupta*

*to the*



**Department of Computer Science and Engineering**

Indian Institute of Technology Kanpur

January 2015

# CERTIFICATE

This is to certify that the work contained in this thesis entitled “ *Contact Lenses Detection using Local Phase Quantization and Binary Gabor Pattern* ” by *Lovish (Y9227309)* has been carried out under my supervision and this work has not been submitted elsewhere for a degree.

January 2015

Phalguni Gupta

Department of Computer Science and Engineering

Indian Institute of Technology Kanpur

Kanpur, India

# Contents

<b>Acknowledgments</b>	<b>ix</b>
<b>Abstract</b>	<b>xi</b>
<b>1 Introduction</b>	<b>1</b>
1.1 Human Iris Anatomy . . . . .	1
1.2 Contact Lens . . . . .	2
1.3 Problem Statement . . . . .	4
1.4 Motivation . . . . .	4
1.5 Iris Recognition System . . . . .	5
1.6 Outline of the thesis . . . . .	8
<b>2 Related Work</b>	<b>10</b>
<b>3 Background</b>	<b>14</b>
3.1 Sobel Filter . . . . .	14
3.2 Hough Transform . . . . .	16
3.3 Integro-differential Operator . . . . .	17
3.4 Gray Level Co-occurrence Matrix . . . . .	18

3.5	Local Binary Patterns (LBP)	19
3.6	Binary Gabor Pattern	20
3.7	Binary Statistical Image Features	23
3.8	Local Phase Quantization	25
3.9	Support Vector Machine	26
3.10	Ordinal Relationship	28
3.11	Gabor Filters	29
<b>4</b>	<b>Effect of Contact Lenses on Iris Recognition</b>	<b>31</b>
4.1	Dataset	32
4.2	Experimental Section	33
4.2.1	Performance Metrics	33
4.2.2	Results for Iris Template Matching	36
<b>5</b>	<b>Cosmetic Contact Lens Detection</b>	<b>44</b>
5.1	Preprocessing	44
5.2	Cosmetic Lens Detection	45
5.2.1	Training	46
5.2.2	Prediction	46
5.3	Lens Detection Results	48
5.3.1	Performance Metrics	48
5.3.2	Experimental Results	50
<b>6</b>	<b>Conclusions and Future Work</b>	<b>54</b>
6.1	Conclusions	54
6.2	Future Work	55

# List of Figures

1.1	The Human Iris . . . . .	2
1.2	Type of Contact Lens . . . . .	3
1.3	Cosmetic Lenses from Different manufacturers . . . . .	3
1.4	Two Modes of Matching . . . . .	6
1.5	Camera and Setup used in IITK Contact Lens Image Acquisition[1]	6
1.6	Iris Preprocessing Pipeline . . . . .	7
1.7	Causes of Occlusion . . . . .	7
1.8	Iris Recognition System . . . . .	9
2.1	Poor Quality Iris Images . . . . .	11
3.1	Sobel Edge Detection on Iris image . . . . .	15
3.2	Circular Hough Transform . . . . .	16
3.3	Integro-differential Operator . . . . .	17
3.4	LBP value computation . . . . .	19
3.5	Circularly symmetric LBP neighborhoods for different ( $n, d$ ) . . . . .	21
3.6	BGP value computation . . . . .	22
3.7	8 9x9 Features learnt using ICA [2] . . . . .	24
3.8	Support Vectors in SVM . . . . .	27

3.9	An ordinal filter . . . . .	29
3.10	Gabor Response for a Normalized Iris . . . . .	30
4.1	Structure of Contact Lens dataset . . . . .	32
4.2	Images from different datasets . . . . .	37
4.3	ROC Curve and Determination of EER . . . . .	38
4.4	Genuine Impostor Plots . . . . .	38
4.5	Receiver Operating Characteristic(ROC) Curves . . . . .	41
4.6	ROC Curve taking "No-Lens" Class as gallery Set . . . . .	42
4.7	Genuine Inposter Plots . . . . .	43
5.1	Iris Preprocessing . . . . .	45
5.2	Lens Detection Process . . . . .	46
5.3	Sample Images from UND Contact Lens dataset . . . . .	49
6.1	Example Images with Soft Lens in IITK Dataset . . . . .	56
6.2	Unconventional Lenses Available in the Market [3] . . . . .	56

# List of Tables

4.1	IITK Contact Lens Dataset Summary . . . . .	33
4.2	IITD Contact Lens Dataset Summary . . . . .	33
4.3	Performance Degradation due to use of Contact Lens . . . . .	39
5.1	UND Contact Lens Dataset Summary . . . . .	48
5.2	CCR and FAR across Various Texture Description Techniques . . .	51

# List of Algorithms

1	Local Phase Quantization Feature Extraction . . . . .	47
2	Binary Gabor Pattern Feature Extraction . . . . .	52

# Acknowledgments

I would like to take this opportunity to thank the people who have helped me in the preparation of this thesis. Firstly, I would like to thank my parents without whose blessings and support this thesis would not have been possible.

I would like to sincerely thank my thesis adviser Prof. Phalguni Gupta for his valuable inputs from time to time. I am also grateful to him for giving me full freedom in deciding the topic of my interest. The biometrics research laboratory with all the necessary equipment is a great place to work.

I express my sincere thanks to Mr. Aditya Nigam for guiding me whenever I was stuck at some point. I would also like to thank my lab mates Ajmera, Aman, Satyendra, Gunakesh, Yogi and Suresh for providing healthy support which kept me motivated all the time.

Lastly, I must confess I will never be able to thank IITK enough for the excellent opportunities, academic environment and research facilities which have inspired me to work hard for this thesis.

Lovish

*Dedicated to the Research  
Community*

# Abstract

Iris has emerged as a prime biometric trait in the past decade. It has been deployed in large scale biometric identification programs such as UIDAI in India, RIC in Brazil and EIDA in UAE. One of the reason behind use of iris is its resistance to circumvention. Unfortunately sensor level spoofing attacks such as use of printed iris, artificial eyeballs and contact lenses have raised the issue of iris liveness detection in the biometric community.

In this thesis, a survey regarding the effects of contact lens on iris recognition is accomplished. A dataset containing images of subjects wearing two types of contact lenses has been constructed. The effects of soft and cosmetic contact lens on iris recognition techniques has been described. A cosmetic contact lens detection scheme using fusion of Local Phase Quantization and Binary Gabor Pattern has been proposed. Experimental results on the IITK dataset and publicly available IIITD Cogent, IIITD Vista and UND datasets show that the current approach outperforms previous lens detection techniques for three of the four datasets in terms of Correct Classification Rate and False Acceptance Rate.

# Chapter 1

## Introduction

Iris based biometric systems have gained lot of popularity in last decade because of their low invasiveness and resistance to circumvention. However, contact lenses which are worn on iris to correct vision partially obfuscate iris texture and make the system prone to circumvention. This thesis deals with the problem of quantifying the effect of two types of contact lenses on iris recognition systems and detection of cosmetic contact lenses. It has proposed a lens detection scheme which is based on the fusion of Local Phase Quantization and Binary Gabor Pattern. Experimental results on three datasets show that it outperforms texture detection techniques such as GLCM and LBP.

### 1.1 Human Iris Anatomy

Iris is an annular portion of eye lying between pupil and sclera as shown in Figure 1.1(b). It contains significant points such as freckles, rifts, edges, crypts etc. Flom and Safir [4] have shown that iris texture is unique for each individual.

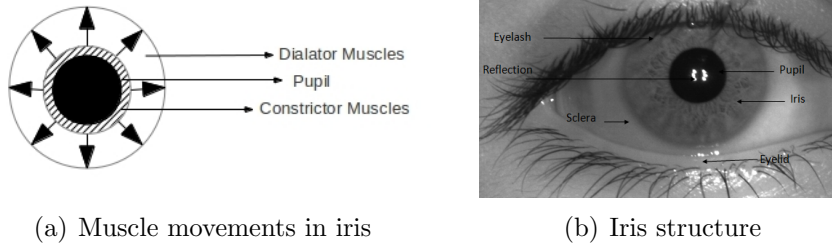


Figure 1.1: The Human Iris

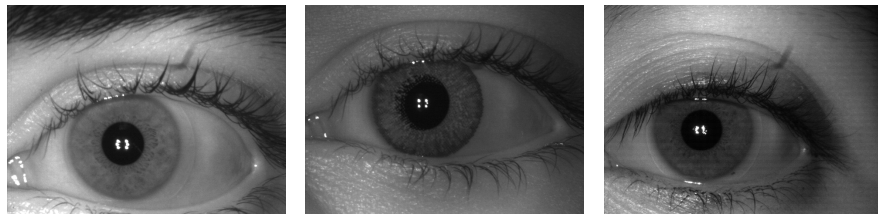
The characteristics of a human iris remain stable with time and it is very difficult to modify them surgically. Sphincter and dilator muscles control the amount of light entering the iris. For a small pupil, the sphincter muscle contracts and the dilator muscle relaxes while the sphincter muscle relaxes and dilator muscle contracts for a large pupil. The location of dilator and sphincter muscles within the iris is shown in Figure 1.1(a).

## 1.2 Contact Lens

Contact lens is a medical device worn to correct vision problems such as myopia, hyperopia and astigmatism. Broadly, contact lenses can be classified into two categories based on their appearance - soft lens and cosmetic lens. Soft lenses are transparent in nature and are used to correct vision problems such as myopia and hypertropia. Cosmetic contact lenses have a pattern printed on them that changes the appearance of human iris apart from correcting vision of the subject. The texture printed on the cosmetic contact lens partially obfuscates the original iris pattern. A less popular type includes Toric contact lenses which have different focal lengths along two perpendicular axes and align themselves according to the

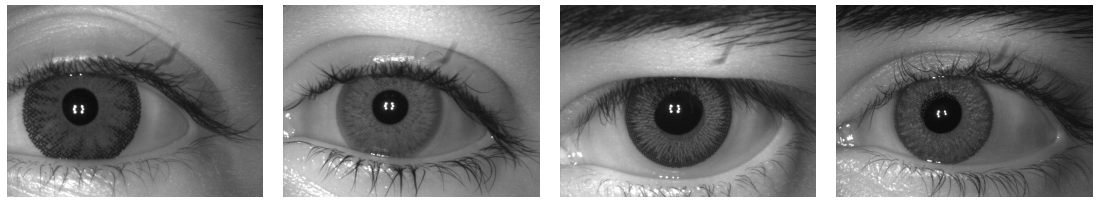
user's refractive error. Different types of contact lenses are shown in Figure 1.2.

Recently cosmetic contact lenses have started to gain popularity among people who wish to avoid using eyeglasses and enhance the aesthetic appearance of their eyes. Moreover, texture of cosmetic contact lens varies widely and depends on the manufacturer of the lens as shown in Figure 1.3.



(a) Transparent Contact Lens    (b) Cosmetic Contact Lens    (c) Toric Contact Lens

Figure 1.2: Type of Contact Lens



(a) OxyColor Lens    (b) Flamboyent Lens    (c) O2Max Lens    (d) Freshlook Lens

Figure 1.3: Cosmetic Lenses from Different manufacturers

### 1.3 Problem Statement

Suitable encodings of the iris texture have been used to identify individuals with good accuracy [5]. These methods perform well in a controlled environment in the absence of external variations. The problem of spoofing through contact lens has

not been addressed explicitly by these methods. To evaluate the effects of contact lens on iris recognition, results of cosmetic and soft lens for three techniques on three datasets have been quantified. This thesis has dealt with the problem of cosmetic lens detection which plays an important role in strengthening the non-invasive character of an iris recognition system.

## 1.4 Motivation

Although iris is a stable, universal, unique and non-invasive biometric trait, the use of contact lens while enrollment or identification can help an individual circumvent the underlying recognition algorithm in a biometric system. It can help a criminal in evading detection, creating synthetic identity or even impersonating a target identity by using a custom made cosmetic contact lens. Moreover, contact lenses are available easily and cheaply in the market today which increases the odds of their use against spoofing iris biometric systems. This motivation behind this work is to find a comprehensive texture descriptor which is suitable for cosmetic lens detection.

## 1.5 Iris Recognition System

Iris based biometric system consists of an enrollment stage where the acquired image is preprocessed and feature encoding is carried out. This leads to the creation of iris template which is enhanced to highlight certain patterns in the iris. Like any other biometric system, the iris biometric system is operated in two modes :-

- *Verification* is a one-to-one matching when iris biometric template of the

probe is matched with a specific stored template to verify if the individual is the person whose identity is being claimed.

- *Identification* is one-to-many matching when the iris biometric template of probe is matched with every template stored in the dataset to determine the identity of an individual. More time is consumed in identification mode as multiple matches are performed for each template. Figure 1.4 illustrates the above two modes.

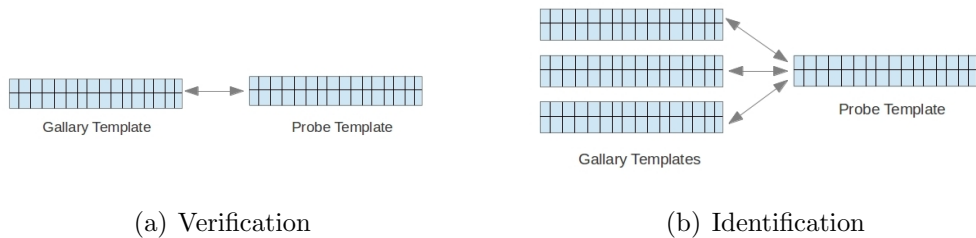


Figure 1.4: Two Modes of Matching

1. **Image Acquisition :** The camera used in acquisition of images makes use of automatic focus adjustment. Subject holds the camera in one hand and is required to move the camera according to the color of LED indicator. Red and blue color indicates that the iris of subject is nearer and further from the camera respectively. Green LED indicates correct distance and an image is taken automatically by the camera at that instant. The camera used and the setup is shown in Figure 1.5. All images are captured in Near Infra Red NIR spectrum ie 700-900 nm because the structural details of darker irises appear much better in NIR than visible range.

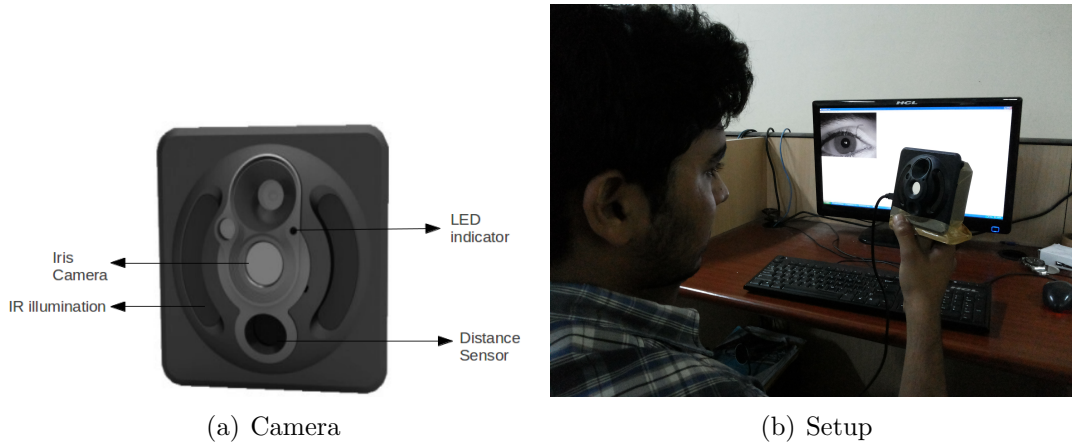


Figure 1.5: Camera and Setup used in IITK Contact Lens Image Acquisition[1]

**2. Iris Preprocessing:** Region of interest from the iris image is extracted to find the desired features. The pupil and iris boundary are detected in acquired image. Then the annular area between them is segmented and normalized to form a rectangular iris template.

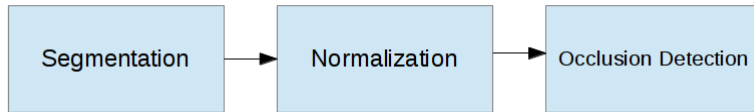


Figure 1.6: Iris Preprocessing Pipeline

- *Segmentation and Normalization:* In this step, both inner and outer boundaries of iris region are detected. Their centers, along with the respective radii are stored for segmentation. Finally, the iris image is normalized by transforming the annular area from Cartesian to polar coordinates. Normalization ensures a uniform size for all iris templates enrolled in the dataset.

- *Occlusion detection:* Eyelids, eyelashes and specular reflections need to be detected and masked in the templates to be matched. Only the non-occluded regions of iris are considered for matching. Figure 1.7 shows the main causes of occlusion in iris.

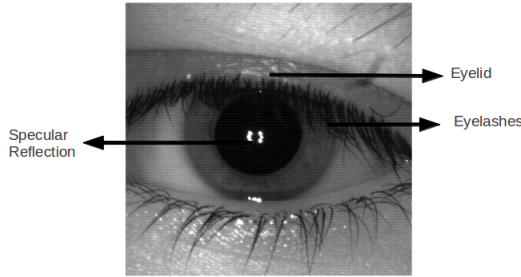


Figure 1.7: Causes of Occlusion

3. **Feature Extraction:** Appropriate techniques is used to encode the iris texture to create a template which represents the iris image acquired in the first step.

4. **Template Matching:** The probe template formed in the third step is compared against all the stored templates in the dataset. Best match is decided on the basis of either similarity or dissimilarity score.

For verification, a single match needs to be performed. A threshold based on the dataset is used to decide weather the probe image belongs to a genuine or impostor.

## 1.6 Outline of the thesis

In this thesis, the effect of two major types of contact lenses is evaluated across three datasets. Three iris recognition approaches using log-gabor filter, gabor filer, local binary patterns and relational measures are used to quantify the degradation in performance of iris recognition system in the presence of soft lens and cosmetic contact lens. Further we propose a cosmetic lens detection approach based on Local Phase Quantization(LPQ) and Binary Gabor Pattern(BGP). Using this approach, a new iris recognition system is proposed which is summarized in Figure 1.8.

The thesis is divided into six chapters. A survey of the work done on iris recognition and anti-spoofing measures is described in Chapter 2. Some techniques that act as a building block of proposed approach are introduced in Chapter 3. Next Chapter describes the effect of presence of soft and cosmetic contact lens on iris recognition techniques. Methods used for detection of contact lens on iris recognition and results are described in Chapter 5. Finally, the conclusion and future work is described in Chapter 6.

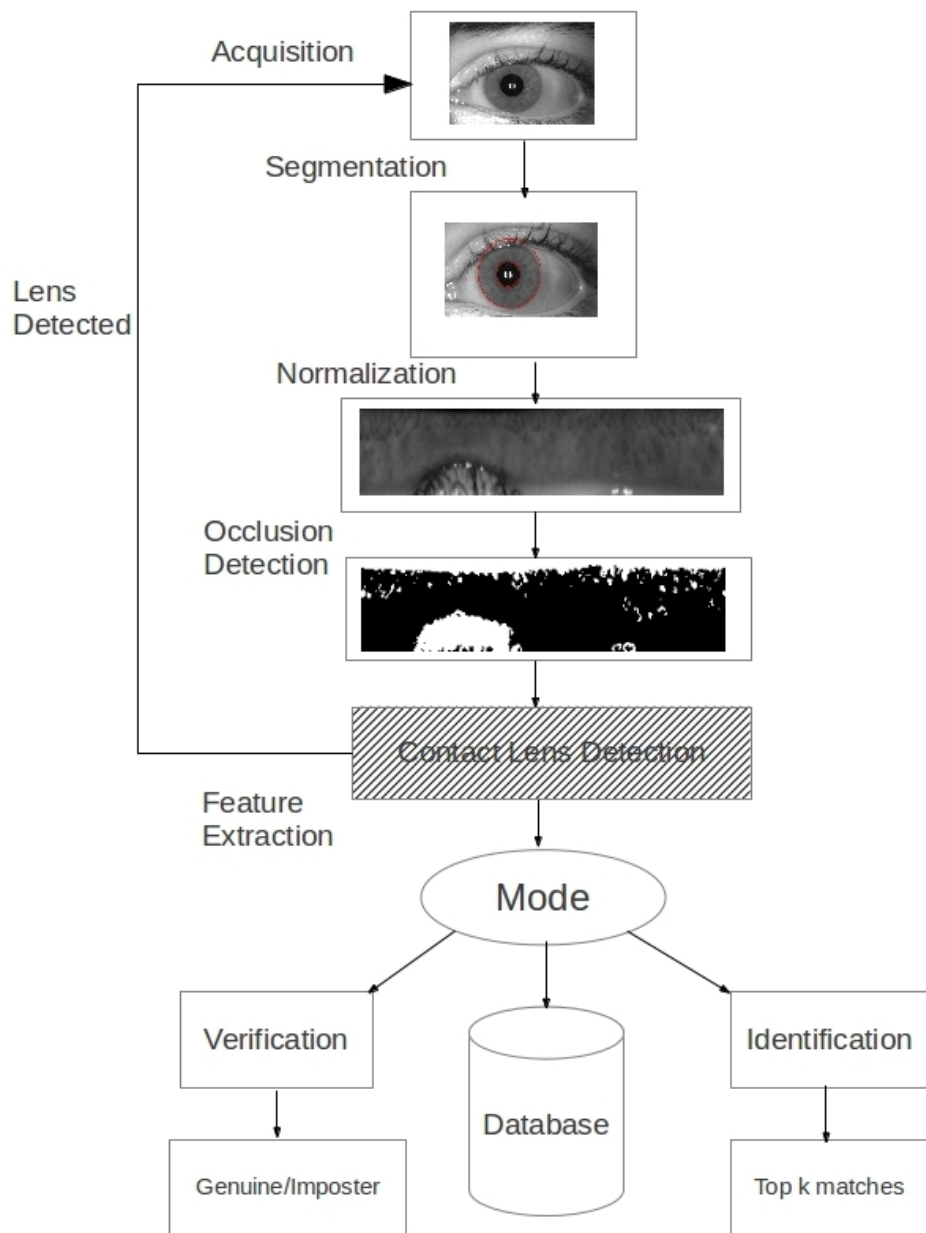


Figure 1.8: Iris Recognition System

# Chapter 2

## Related Work

The first iris recognition system has been proposed by Daugman [5]. The segmentation of inner and outer boundary of iris has been carried out by the use of integro-differential operator. Features have been extracted using two-dimensional Gabor wavelets. Finally, the feature template has been defined as a sequence of bits derived through the quantized phase information of the local iris texture. There exist many iris recognition systems which are based on the concept of [5]. In [6], Daugman has improved upon the previous approach by devising a more flexible method in detecting inner and outer boundary. Fourier-based methods in projective geometry have been used to counter off-axis iris gaze. An example of off-angle iris is shown in Figure 2.1(d).

There exist iris acquisition systems varying in degree of intrusiveness and image quality. Major work in this area focuses on reducing user's cooperation, increasing operating distance and extending the depth of field of acquisition system. "Iris on the Move" [7] and "Eagle-Eyes" [8] are prototype systems which can be used to acquire two iris images of a subject with a large distance between subject and the

camera. Many mobile iris acquisition are considered safe to authenticate for online transactions [9]. Metrics such as focus blur, motion blur, degree of occlusion, off-angle gaze are used to determine the quality of iris templates. Kalka et al [10] have shown that incorporating these quality matrices improves the performance of iris based biometric systems. If the quality of the acquired iris images is found to be poor, user can be asked to re-enroll in the dataset. Some poor quality iris images are shown in Figure 2.1.

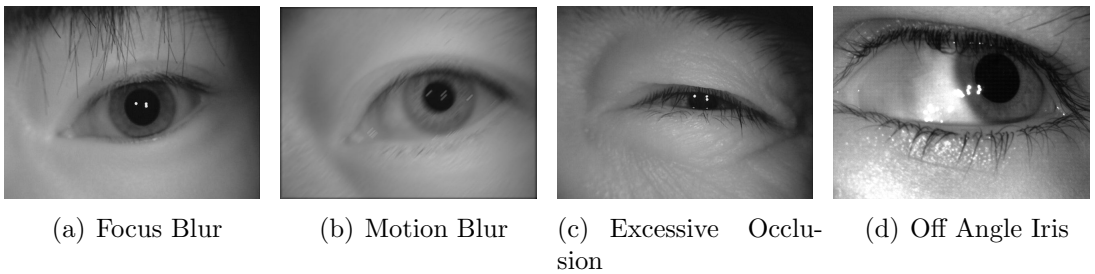


Figure 2.1: Poor Quality Iris Images

For iris segmentation, techniques based on Hough transform has been proposed in [11, 12]. An iris segmentation approach by pulling and pushing has been proposed in [13] where the edge points of iris boundaries are iteratively refined in a way as done by restoring forces in Hooke's law [14].

Occlusion from eyelids, eyelashes and specular reflection degrades the matching process as unwanted features from these portions appear in iris template. In [15], accurate eyelid localization has been carried out through coarse to fine level parabola fitting. Eyelashes are categorized as "mixed" or "separable" based on the area occluded by them. Techniques using gray-level co-occurrence matrix (GLCM) have been used to classify iris image into skin, sclera, pupil and iris based on their texture [16].

Contact Lens detection has been an emerging area of research in iris recognition since the past few years. A method based on the theoretical position and distances between Purkinje Images has been proposed in [17]. Stereo Imaging has been used in [18] where the presence of lens is found by estimating the surface shape of iris region. Despite being accurate, both the methods need additional hardware to detect contact lens. Daugman [19] has used Fast Fourier Transform (FFT) to detect spatial pattern on a dot-matrix printed lens. He et al[20] have used LBP histograms as features and adaboost technique to find most discriminative features for contact lens detection. Komulainen et al [21] have proposed a generalized lens detection technique using statistically independent filters. Sun et al [22] have used hierarchical visual codebook model to encode distinctive and robust texture primitives in cosmetic lenses. It achieved a 100% correct classification rate on a proprietary dataset.

Generation of iris template has been carried out using various methods. In [23] the quantized phase data derived from convolving normalized iris with one-dimensional Gabor filter has been used to generate iris template. Another approach using zero crossings of DCT coefficients has been proposed in [24]. Ordinal methods proposed in [24] have used the sign of relative intensity between two regions of image to generate a binary template. Local Binary Patterns and its variants have also been used to encode iris texture. Uniform LBP histograms generated from non-overlapping blocks have been used to create a global representation of normalized iris image in [25]. LBP in [26] is combined with blob extraction through LoG filter leading to a hybrid approach accounting for both bright or dark areas along with iris texture. Nigam et al [27] have used fusion of a block level variant of local binary pattern and relational measures to obtain a

feature template.

# Chapter 3

## Background

This chapter describes the baseline concepts used in designing our system. Sobel operator which gives approximate gradient values at all pixels of an image has been described in this chapter. The circular shapes in sobel edge map can be found out by using Hough transform and Integro-Differential operator. Their shapes are used in detecting inner and outer boundaries of iris respectively. Gray level co-occurrence matrix, Local Binary pattern, Binary Gabor Patterns, Binary Statistical Image Features and Local Phase Quantization have been used for constructing feature histograms. Scalar Vector Machine (SVM) has been used to classify the feature vectors into cosmetic lens or no lens class. Gabor filtering presented in this chapter has been used for matching iris features.

### 3.1 Sobel Filter

Sobel filters calculate the approximation of gradients in both horizontal and vertical directions. Each image is convolved with two  $3 \times 3$  kernels to get horizontal

gradient  $S_x$  and vertical gradient  $S_y$ .

$$S_x = \begin{bmatrix} -1 & 0 & +1 \\ -2 & 0 & +2 \\ -1 & 0 & +1 \end{bmatrix} * X \quad S_y = \begin{bmatrix} -1 & -2 & -1 \\ 0 & 0 & 0 \\ +1 & +2 & +1 \end{bmatrix} * X$$

where  $*$  stands for convolution operator. It is assumed that  $x$ -coordinate is increasing in right direction and  $y$ -coordinate is increasing in downward direction. The magnitude  $S(x, y)$  and direction  $\theta(x, y)$  of gradient at  $(x, y)$  are given by the Equations 3.1 and 3.2 respectively.

$$S(x, y) = (S_Y^2(x, y) + S_X^2(x, y))^{\frac{1}{2}} \quad (3.1)$$

$$\theta(x, y) = \tan^{-1} \left( \frac{S_Y(x, y)}{S_X(x, y)} \right). \quad (3.2)$$

An application of sobel filter on an iris image is shown in Figure 3.1.

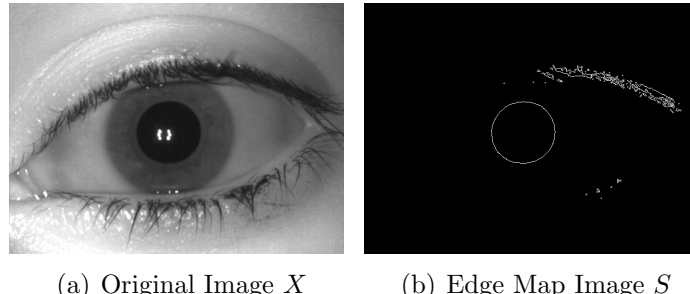


Figure 3.1: Sobel Edge Detection on Iris image

## 3.2 Hough Transform

The motive of Hough transform is to find instances of circular shape in an iris image. This problem can be formalized as :-

$$V(a, b) = |\{(x, y) \in E : (x - a)^2 + (y - b)^2 = R^2\}| \quad (3.3)$$

$$(x_c, y_c) \leftarrow argmax_{(a,b)}(V) \quad (3.4)$$

where  $E$  is the edge map shown in Figure 3.2(a) on which the circle is to be detected,  $(a, b)$  is the candidate center of circle and  $V(a, b)$  are votes corresponding to the center. To find the circle present in an iris image, an edge map  $E$  of

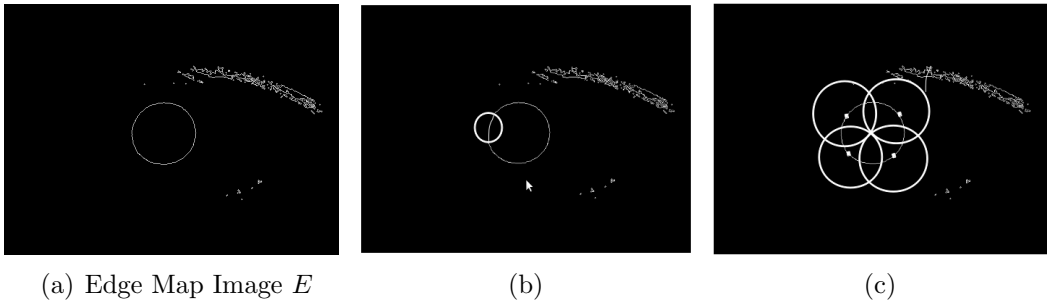


Figure 3.2: Circular Hough Transform

image is generated. For each of the edge pixels in  $E$ , locus of candidate centers is calculated. It is considered to be centered at edge pixel and having radius  $R$  as shown in Figure 3.2(b). Each edge points adds a single vote to candidate center point. Finally, as shown in Figure 3.2(c) the candidate center with maximum votes is chosen as center for the circle. Although Hough transform follows a brute force technique for detecting shapes, it is robust to noisy points and offers much flexibility in shape detection.

### 3.3 Integro-differential Operator

If the edge map is not obtained properly by the Sobel filter, hough transform fails to detect circular shape of pupil and iris. In such a case, integro-differential operator proposed by Daugman [28] can be used to obtain a robust method to detect circles. It aims to maximize the intensity gradient along the circular contour.

Mathematically, it is defined as :-

$$\max_{(r, x_c, y_c)} \left| G_\sigma(r) * \frac{\partial}{\partial r} \oint_{(r, x_c, y_c)} \frac{I(x, y)}{2\pi r} ds \right| \quad (3.5)$$

where  $I(x, y)$  is the eye image,  $r$  is the search radius,  $G_\sigma(r)$  is gaussian filter function and  $s$  is the contour of circle defined by  $(r, x_c, y_c)$ . It locates the circle by finding maximum gradient circular contour defined by all candidate centers  $(x_c, y_c)$  and radius  $r$ . The integro-differential operator is used to find the limbic boundary in iris as shown in Figure 3.3.

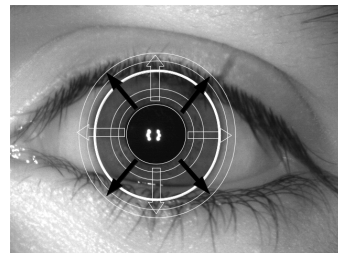


Figure 3.3: Integro-differential Operator

### 3.4 Gray Level Co-occurrence Matrix

A matrix that defines the distribution of co-occurring values at a given offset over a gray scale image is called Gray Level Co-occurrence Matrix (GLCM) [29]. Mathematically, it is given by matrix  $C$  in Equation 3.6.

$$C_{\Delta x, \Delta y}(i, j) = \sum_{p=1}^n \sum_{q=1}^m \begin{cases} 1, & \text{if } I(p, q) = i \text{ and } I(p + \Delta p, q + \Delta q) = j \\ 0, & \text{otherwise} \end{cases} \quad (3.6)$$

where  $n \times m$  denotes the dimensions of image,  $(x, y)$  are intensity values,  $(p, q)$  is the position of a particular pixel and  $(\Delta p, \Delta q)$  is the offset. Generally the co-occurrence matrix is formed for a set of orientations ranging  $(0^\circ, 45^\circ, 90^\circ, 135^\circ)$  at equal offsets to achieve rotational invariant representation of given image. From  $C$ , a general form of gray-tone dependency matrix is obtained for image with gray tone values ranging from 0 to 3 and is represented as  $G$ . An image  $I$  with four grey-tone values ranging from 0 to 3 and corresponding unit offset co-occurrence matrices corresponding to  $I$  are depicted as  $G_0$ ,  $G_{90}$ ,  $G_{45}$  and  $G_{135}$  respectively.

$$I = \begin{bmatrix} 0 & 2 & 3 & 1 \\ 1 & 3 & 0 & 2 \\ 1 & 0 & 3 & 2 \\ 2 & 1 & 3 & 2 \end{bmatrix} \quad G = \begin{bmatrix} (0,0) & (0,1) & (0,2) & (0,3) \\ (1,0) & (1,1) & (1,2) & (1,3) \\ (2,0) & (2,1) & (2,2) & (2,3) \\ (3,0) & (3,1) & (3,2) & (3,3) \end{bmatrix}$$

$$G_0(I) = \begin{bmatrix} 0 & 1 & 2 & 2 \\ 1 & 0 & 1 & 3 \\ 2 & 1 & 0 & 3 \\ 2 & 3 & 3 & 0 \end{bmatrix} \quad G_{90}(I) = \begin{bmatrix} 0 & 2 & 0 & 3 \\ 2 & 2 & 2 & 0 \\ 0 & 2 & 4 & 1 \\ 3 & 0 & 1 & 2 \end{bmatrix}$$

$$G_{45}(I) = \begin{bmatrix} 2 & 0 & 1 & 0 \\ 0 & 0 & 1 & 2 \\ 1 & 1 & 0 & 2 \\ 0 & 2 & 2 & 2 \end{bmatrix} \quad G_{135}(I) = \begin{bmatrix} 0 & 1 & 1 & 2 \\ 1 & 2 & 0 & 0 \\ 1 & 0 & 0 & 1 \\ 2 & 0 & 1 & 2 \end{bmatrix}$$

### 3.5 Local Binary Patterns (LBP)

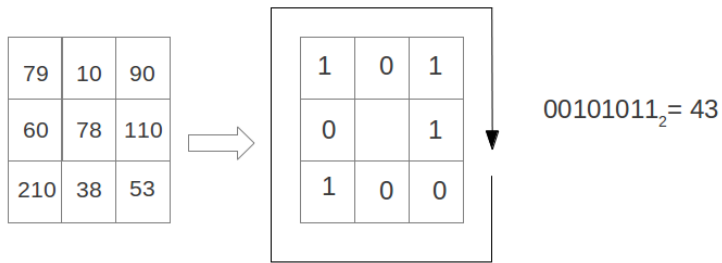


Figure 3.4: LBP value computation

Local Binary Patterns (LBP) [30] consist of thresholding the neighbors of a pixel by its own value followed by a decimal representation of the binary string obtained. In standard LBP, only eight neighbors of a surrounding pixel are considered for comparison. Decimal values are used to create a histogram which acts as a feature to represent the spatial structure. Binary patterns with less than 3 bit transitions are known as uniform patterns. In [30], Ojala et al have shown that uniform patterns consist most of the natural patterns found in textures and rest of the patterns consist of noise.

A LBP histogram  $H$  is created for each normalized iris template. All uniform patterns are assigned different bins whereas the non-uniform patterns are all

mapped to same bin. Hence for a 8-bit greyscale image having intensities in the range of 0-255, 59 bins are used. 58 of these bins correspond to uniform patterns and one bin is allotted to all non-uniform patterns.

For a center pixel, different kind of circularly symmetric regions are chosen depending on the number of pixels  $n$  in neighborhood and distance  $d$  to these pixels. Histograms obtained from different values of  $(n, d)$  as shown in Figure 3.5 can be combined to get a fused multi-scale textural features.

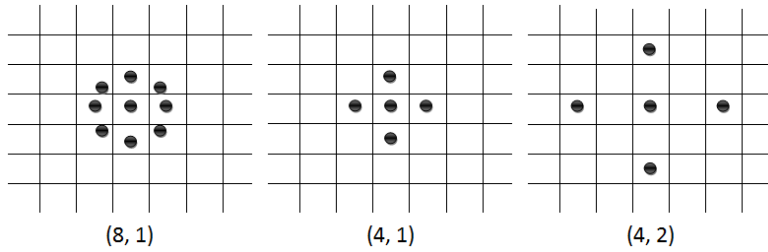


Figure 3.5: Circularly symmetric LBP neighborhoods for different  $(n, d)$

## 3.6 Binary Gabor Pattern

Binary Gabor pattern (BGP) is a texture descriptor inspired by LBP. Instead of binarising based on difference between two pixels as in LBP, BGP uses the difference between two regions for texture description. The real and complex part of gabor filter can be denoted by Equation 3.7 and Equation 3.8

$$g(x, y) = \exp\left(-\frac{1}{2}\left(\frac{(x')^2}{\sigma^2} + \frac{(y')^2}{(\gamma\sigma)^2}\right)\right) \cos\left(\frac{2\pi}{\lambda}x'\right) \quad (3.7)$$

$$g(x, y) = \exp\left(-\frac{1}{2}\left(\frac{(x')^2}{\sigma^2} + \frac{(y')^2}{(\gamma\sigma)^2}\right)\right) \sin\left(\frac{2\pi}{\lambda}x'\right) \quad (3.8)$$

where  $x' = x \cos(\theta) + y \sin(\theta)$  and  $y' = -x \sin(\theta) + y \cos(\theta)$ ,  $\theta$  represents the orientation of the gabor filter with respect to normal,  $\gamma$  denotes the spatial aspect ratio,  $\sigma$  denotes the sigma of Gaussian and  $\lambda$  is the wavelength of the sinusoidal function. The BGP descriptor for an image is obtained by convolving the patches

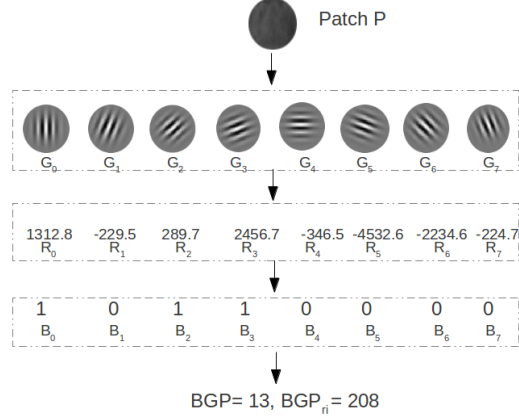


Figure 3.6: BGP value computation

in the image by a filter bank containing gabor filters at 8 different orientations, say ( $G_0$  to  $G_7$ ). The response vector  $R$  is thresholded on the basis of the sign of response and binarized to obtain vector  $B$  which is transformed to a unique number by assigning a unique binomial factor  $2^i$  for bit position  $i$  in  $B = B_i|i = 0..7$ . Hence, the BGP value for patch  $P$  can be given as :-

$$BGP = \sum_{i=0}^{7} B_i \cdot 2^i \quad (3.9)$$

It can be seen that there are  $2^7$  unique values possible from 8 bits of  $B$ . To assign a unique rotation-invariant value to each patch BGP is re-defined as :-

$$BGP_{ri} = MAX(RIGHTSHIFT(BGP, i)|i = 0..7) \quad (3.10)$$

where RIGHTSHIFT performs a circular bitwise right shift on the 8-bit number 7 times and MAX takes the maximum value of all values. Figure 3.6 illustrates the computation of BGP and  $BGP_{ri}$ . The BGP descriptor of an image consists of a histogram formed by concatenating the frequencies of  $BGP_{ri}$  values of several patches within an image.

## 3.7 Binary Statistical Image Features

Texture description approaches such as LBP compute labels for each pixel in its local neighborhood by first convolving the the image with predetermined set of filters and then binarizing the responses. In BSIF texture descriptors, filters are learnt using the statistics of natural images using Independent Component Analysis (ICA).

Let  $n$  be the number of filters of size  $l \times l$ . The filter response for a image patch  $P$  is obtained by

$$R = \sum_{x,y} W(x,y)P(x,y)$$

where  $W$  is a filter matrix of size  $n \times l^2$ . To maximize the statistical independence of  $R$ , the filters in  $W$  are estimated using ICA. The matrix  $W$  is decomposed into two parts - a matrix  $U$  which is found using ICA and  $V$  which performs canonical preprocessing on image patch  $P$ . Canonical preprocessing consists of the following steps :-

- Remove the DC component of patch ie subtract the mean intensity.
- Compute the principal components of all the image patches.
- Retain only first  $n$  components and discard the rest.

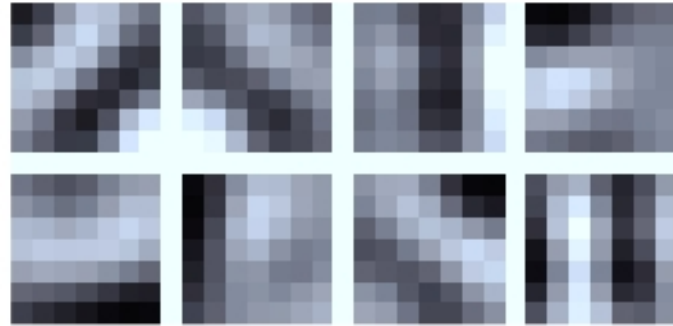


Figure 3.7: 8 9x9 Features learnt using ICA [2]

- Divide the principal components by their standard deviation.

In Equation 3.12,  $T$  represents the preprocessed patch  $P$ :-

$$C = EDE^T \quad (3.11)$$

$$T = (D^{-1/2}E^T)_{(1:n)}P \quad (3.12)$$

where  $D$  is the diagonal matrix obtained through the eigen decomposition of the covariance matrix  $C$  obtained from patch  $P$ .

$$R = WP = U(VP) = UT$$

Finally using  $U$  and  $V$  the filter matrix is obtained as  $W=UV$ . The features learnt by using images provided in [2] are shown in Figure 3.7.

## 3.8 Local Phase Quantization

Techniques such as LBP and BGP concentrate on creating a texture descriptor accommodating certain level of noise, scaling and rotation in the image. However, their descriptor is not robust to image blurring. Local Phase Quantization provides a texture descriptor which is invariant to centrally symmetric blur. Spatial blur in an image can be represented as convolution of an image with a blur function. According to the convolution theorem, the Fourier transform of a convolution in spatial domain can be represented as point wise multiplication in frequency domain. Let  $i, b, l$  represent the original image, blur function and blurred image respectively. In spatial domain, the relationship among them can be described as :-

$$l(x, y) = i(x, y) * b(x, y) \quad (3.13)$$

Let  $I, B, L$  represent the Fourier transforms of original image, blur function and blurred image respectively. In frequency domain, the relationship among them is given by Equation 3.14.

$$L(u, v) = I(u, v) \cdot B(u, v) \quad (3.14)$$

where “.” denotes the point-wise multiplication. The phase relationship can be represented by :-

$$\angle L = \angle I + \angle B \quad (3.15)$$

If the Point Spread Function (PSF) causing blur is centrally symmetric,  $B$  is real valued and  $\angle B$  is either  $0$  or  $\pi$  depending on whether  $B$  is positive or negative.

The phase relationship for centrally symmetric PSF can be simplified as :-

$$\angle L = \angle I \text{ for all } B \geq 0 \quad (3.16)$$

In case of ideal motion and focus blur, the cross section of  $b$  is rectangular [31] and centrally symmetric.  $B$  is represented by *sinc* function containing positive values before the zero-crossing. Thus Equation 3.16 holds true and local phase of pixels in blurred image is equal to local phase of the pixels in original image for 2D-frequencies  $[a, 0]$ ,  $[0, a]$ ,  $[a, a]$  and  $[a, -a]$  where  $a$  is a scalar less than zero-crossing. Real and Complex responses from these four frequencies are concatenated to form a 8-bit vector  $X$ . The coefficients of  $X$  are decor-related using whitening transform for statistical independence. Further these are quantized between values ranging from 0 to 255 using binary coding. Finally, histogram composed of the quantized values is used as feature vector.

### 3.9 Support Vector Machine

Support Vector Machine (SVM) is a supervised learning technique which constructs a hyperplane in higher dimension. The main objective of SVM is to find support vectors and the hyperplane with the largest margin of separation. Let  $m$  be the number of training points belonging to two different classes. This can be described by the following Equation :-

$$D = (x_1, y_1), (x_2, y_2), \dots, (x_m, y_m), \text{where } x_i \in \Re^p \text{ and } y \in -1, 1 \quad (3.17)$$

Support vectors  $S_1$  and  $S_2$  are chosen such that the distance between parallel hyperplanes passing through them is maximized. The problem can be formally described as :-

$$W.x + B = 0, \text{ where } W = \sum_{i=1}^{|S|} \alpha_i y_i x_i \text{ and } |S| \leq n \quad (3.18)$$

Two parallel planes passing through support vectors are given as :-

$$W.x + B = -1 \quad (3.19)$$

$$W.x + B = 1 \quad (3.20)$$

The distance between hyperplanes passing through them is given by  $\frac{2}{\|w\|}$ . To

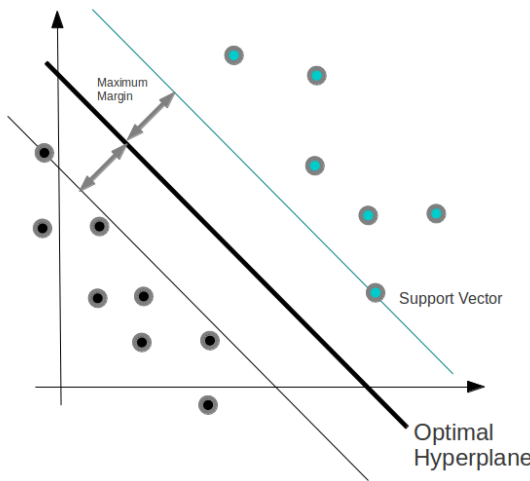


Figure 3.8: Support Vectors in SVM

maximize the distance between the hyperplanes  $\| w \|$  needs to be minimized. The

points in two classes can be represented as :-

$$W.x_i + B \geq 1 \quad (3.21)$$

$$W.x_i + B \leq -1 \quad (3.22)$$

Equations 3.21 and 3.22 can be combined as :-

$$y_i(x_i.W + B) \geq 1 \quad (3.23)$$

Hence the problem reduces to minimizing  $\| W \|$  with the constrained described in Equation 3.23.

## 3.10 Ordinal Relationship

In an iris template, the ordinal relationship between regions proves out to be very discriminative when suitable filters are used. The normalized iris images are convolved with Multilobe Differential Filters (MLDF) and each "ordinal" comparison is encoded as either "0" or "1" bit depending on the sign of response. An example of MLDF is shown in Figure 3.9. Ordinal feature extraction is time efficient because only addition and subtraction operations are involved in encoding ordinal measures. To ensure that there is no correlation between ordinal measures, specifications such as distance, number of lobes, scale and their spatial configuration are adjusted. Hamming distance [32] is used to quantify dissimilarity between two templates. Simple gaussian filters are used to obtain convoluted responses from normalized iris in [28]. These responses are compared and encoded into Relational

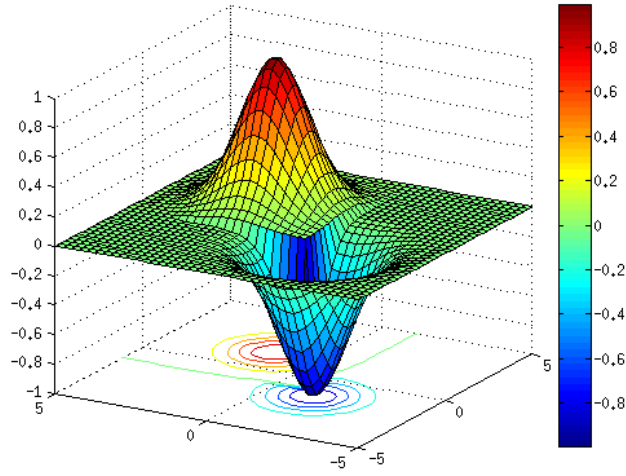


Figure 3.9: An ordinal filter

Measures ( $RM$ ) template.

### 3.11 Gabor Filters

Gabor filters have been used with great success for texture analysis problems. Convolution with Gabor filters is known to be similar to perception in human visual system. Normalized iris image  $N$  can be represented in spatial coordinates  $(r, \theta)$ . The Gabor filter is defined as :-



(a) Real Response



(b) Imaginary Response

Figure 3.10: Gabor Response for a Normalized Iris

$$G(r, \theta) = e^{-i\omega(\theta-\theta_0)} \times e^{-(r-r_0)^2/\alpha^2} \times e^{-(\theta-\theta_0)^2/\beta^2} \quad (3.24)$$

where  $(r_0, \theta_0)$  specify spatial position in the image and  $(\alpha, \beta)$  represent the effective width and length respectively. The 2D filter is convolved with normalized image  $N$  for every pixel  $(r, \theta)$  and two values are obtained. The values obtained are binarized with threshold 0 and two vectors  $b_{Re}$  and  $b_{Im}$  are obtained for each image. Figure 3.11 shows the real and imaginary response when the iris image is convolved with Gabor filter.

# Chapter 4

## Effect of Contact Lenses on Iris Recognition

This chapter discusses experiments that quantify the effects of contact lens on existing iris recognition systems. Template matching has been carried out by iris recognition techniques proposed in [23], [5] and [27]. Log-Gabor and Gabor filtering based approach have been used in [23] and [5] respectively fusion of a block level variant of local binary patterns and relational measures to extract features have been used in [27]. Experiments prove that a user wearing contact lens degrades the overall performance irrespective of the underlying matching algorithm.

Dataset used for the experiments consist of three image classes – cosmetic lens, soft lens and no lens. Each dataset used has the structure as shown in Figure 4.1. It is divided into gallery and probe sets. Each iris image belongs to only one of these sets. The scores obtained from matching probe image with gallery images are used to analyze the effectiveness of the approach in discriminating intra-class and inter-class iris images.

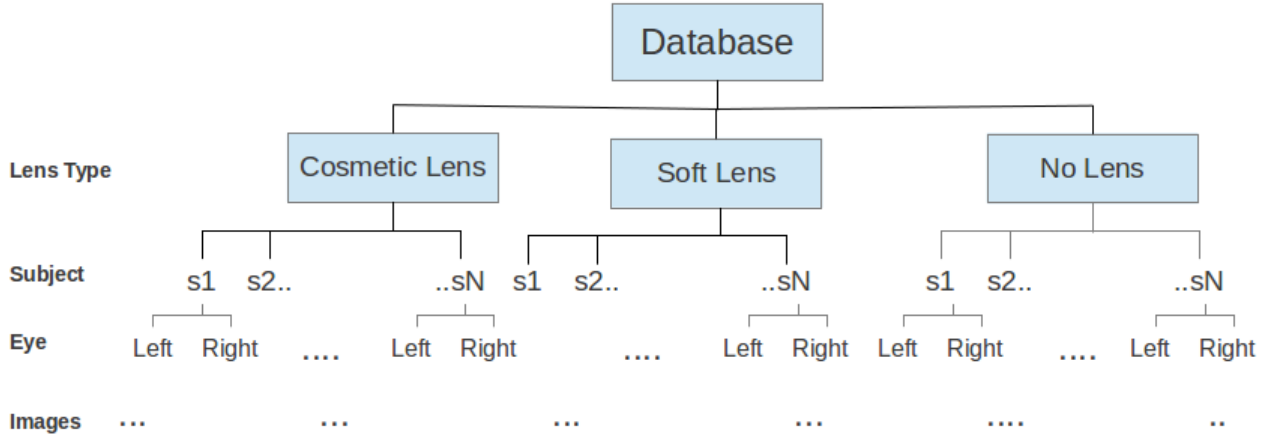


Figure 4.1: Structure of Contact Lens dataset

## 4.1 Dataset

Two different datasets are used to evaluate the effect of contact lenses on iris recognition performance - IITK Contact lens dataset and IIITD Contact lens dataset [33, 34]. The IITK contact lens dataset consists of images taken by Vista Imaging FA2 iris sensor. IIITD contact lens dataset consists of images captured from two different sensors - Vista Imaging FA2 and Cogent Dual Iris Sensor. Both these datasets contain iris images in three scenarios: (a) wearing cosmetic contact lens, (b) wearing soft contact lens, (c) wearing no contact lens. IITK Contact lens dataset has been acquired in a single session in an indoor environment. There are three classes in the dataset [‘C’, ‘N’, ‘Y’] corresponding to contact lens, no lens and soft lens respectively. Data is collected for 100 different iris classes from 50 individuals. Since each eye has its unique pattern, left and right iris from the same subject are considered to be belonging to a different class [35]. The details about this dataset are presented in Table 4.1.



(a) IITK Contact Lens dataset



(b) IIITD Vista Contact Lens dataset



(c) IIITD Cogent Contact Lens dataset

Figure 4.2: Images from different datasets

<b>Types of Contact Lens</b>	Cosmetic lens, Soft lens and no lens
<b>Cosmetic Lens Manufacturers</b>	CibaVision, Flaymboyent, Oxycolor, O2Max
<b>Cosmetic Lens Color</b>	Hazel, Green, Blue, Gray
<b>Soft Lens Manufacturers</b>	Bausch & Lomb, Johnson & Johnson
<b>Iris Sensor</b>	Vista Imaging FA2
<b>Images per class</b>	C:4218, N:4551, Y:4054
<b>Minimum images per eye class</b>	20
<b>Total Images</b>	12823

Table 4.1: IITK Contact Lens Dataset Summary

IIITD contact lens dataset has been collected through two different sensors. Vista Sensor captures image of single iris whereas Cogent sensor captures the

images of both the irises simultaneously. Similar to IITK dataset, there are three iris classes corresponding to cosmetic lens , soft lens and no lens. Details about *IITD* contact lens dataset are presented in Table 5.1.

<b>Types of Contact Lens</b>	Cosmetic lens, Soft lens and no lens
<b>Lens Manufacturers</b>	CibaVision, Bausch and Lomb
<b>Cosmetic Lens Color</b>	Hazel, Green, Blue, Gray
<b>Iris Sensor</b>	Vista Imaging, Cogent
<b>Images per class (Cogent Sesnor)</b>	C:1160, N:1163, Y:1143
<b>Images per class (Vista Sensor)</b>	C:1005, N:1000, Y:1010
<b>Minimum images per eye class</b>	5
<b>Total Images</b>	6570

Table 4.2: IITD Contact Lens Dataset Summary

## 4.2 Experimental Section

This section describes the effect of contact lens on three different matching schemes employed in iris recognition systems. The performance metrics in section 4.2.1 quantify the results in 4.2.2.

### 4.2.1 Performance Metrics

#### 4.2.1.1 *CRR*

While using the biometric system in identification model, the template of the probe image is compared with all the templates of gallery images. Correct Recognition Rate (CRR) is the defined as the percentage of probe images whose matching score is maximum (in case of similarity score) or minimum (in case of dissimilarity score) with a gallery image belonging to the same class as the probe. CRR can be

defined as :-

$$CRR = \frac{\sum_{i=1}^N EQUAL(Subject(Best\ match(i)), Subject(i))}{N} \times 100 \quad (4.1)$$

where  $EQUAL(a,b)$  is 1 if a is same as b otherwise 0. All the images in gallery are compared with probe image of subject  $i$ . CRR gives the accuracy with which an pre-enrolled subject's identity can be correctly determined with the system.

#### 4.2.1.2 **EER**

During verification, a single match is required to authenticate the subject based on the score obtained when probe image of a subject is matched with gallery image of the same subject. The following metrics are used in case of verification :-

1. **False Accept Rate (FAR):** The iris recognition system is operated at certain fixed threshold  $t$  determined initially. If dissimilarity score is less than  $t$ , the probe image is assumed to be of the same subject whose identity is being claimed. FAR , defined at a certain threshold  $t$  is the percentage of impostors accepted as genuine as the matching score lies within the threshold.
- At a threshold  $t$ , the FAR is defined as :-

$$FAR(t) = \frac{\text{Number of impostor falsely accepted as genuine}}{\text{Total number of impostor matchings}} \times 100 \quad (4.2)$$

2. **False Reject Rate (FRR):** FRR is defined as the percentage of genuine matches rejected as impostors because their dissimilarity score are greater

than the threshold  $t$ . The FRR is defined by :-

$$FRR(t) = \frac{\text{Number of genuine falsely rejected as impostor}}{\text{Total number of genuine matchings}} \times 100 \quad (4.3)$$

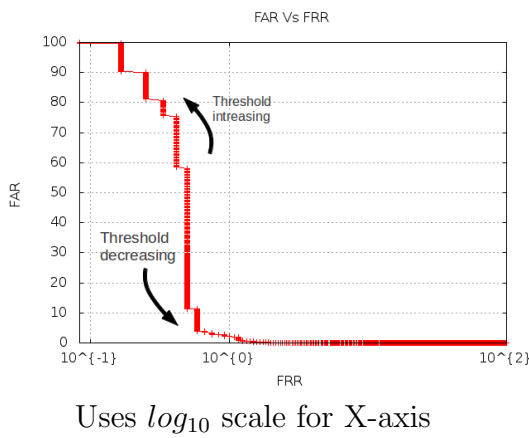


Figure 4.3: ROC Curve and Determination of EER

### 3. Receiver Operating Characteristic (ROC):

For every possible value of threshold  $t$ , values of FAR and FRR are computed. As the threshold is decreased, more genuine users are falsely rejected as well as more impostors are genuinely rejected *ie* FRR increases and FAR decreases. When the threshold  $t$  is increased, FAR increases and FRR decreases. ROC curve is the plot of  $FAR(t)$  and  $FRR(t)$  at varying threshold  $t$ . Figure 4.3 shows the effect of increase and decrease of threshold  $t$  on FAR and FRR.

### 4. Equal Error Rate (EER):

The point where FAR equals FRR is chosen as optimum threshold. FAR or FRR at this point is known as EER. Low

EER value implies superior performance of biometric system.

**5. Genuine-impostor Plot:** Frequency of genuine and impostor comparison scores are plotted against dissimilarity score to get the genuine impostor plot. For an ideal biometric system, the genuine score distribution should be completely separate from the impostor score distribution as shown in Figure 4.4(a). However, in every biometric systems there is some overlap between the two plots as shown in Figure 4.4(b).

As shown in Figure 4.4(c), if the threshold is between  $t_1$  and  $t_2$  say  $t_0$ , there is a possibility of error on classification of subjects. The probe images between  $(t_1, t_0)$  may be misclassified as genuine and those between  $(t_0, t_2)$  may be misclassified as probe subjects.

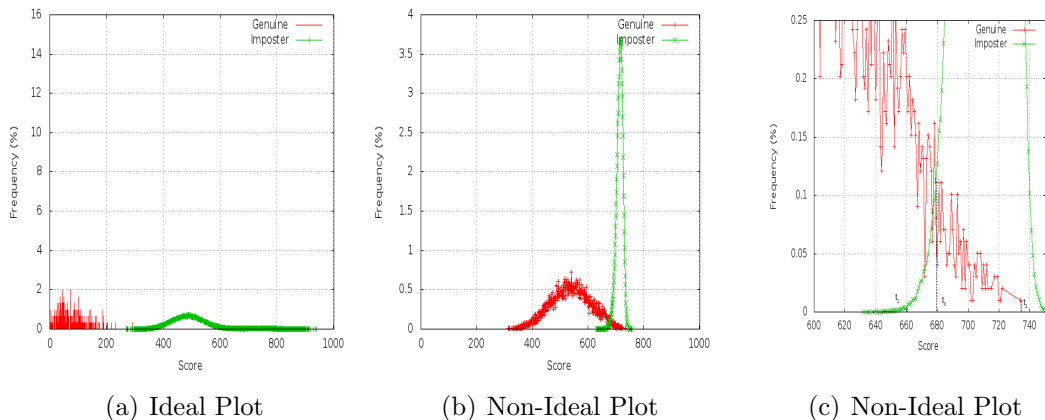


Figure 4.4: Genuine Impostor Plots

#### 4.2.2 Results for Iris Template Matching

Each image is first segmented using technique described in [36] and then normalized according to Daugman's rubber sheet model [5]. Features are extracted from the normalized iris images using iris recognition techniques proposed in Daugman [19], Masek [23] and Nigam et al [27]. All experiments have been conducted on a Intel Xeon E5420 2.80 GHz processor with 4 GB RAM and 64-bit operating system.

In IITK contact lens dataset, minimum number of images present per eye class is 20. 10 images of each class are taken as gallery and rest are taken as probe images. Minimum number of images per eye class is five for both IIITD Vista and IIITD Cogent contact lens dataset. Three of them are taken as gallery and rest 2 are taken as probe for identification and verification experiments. Matching results for three datasets are summarized in Table 4.3.  $D_{CRR}$  and  $D_{EER}$  are for a lens type has been evaluated as follows :-

$$D_{CRR} = CRR(No - No) - CRR(No - Lenstype) \quad (4.4)$$

$$D_{EER} = EER(No - Lenstype) - EER(No - No) \quad (4.5)$$

Dataset	Technique	Masek[23]				Gabor[5]				BLBP+RMH[27]			
		GC-PC	CRR	$D_{CRR}$	EER	$D_{EER}$	CRR	$D_{CRR}$	EER	$D_{EER}$	CRR	$D_{CRR}$	EER
IITD Cogent [33, 34]	No-No	96.76	-	4.56	-	95.27	-	6.51	-	98.75	-	<b>3.14</b>	-
	No-Soft	96.25	0.51	5.41	0.85	92.75	2.52	6.49	0.02	97.50	1.25	<b>4.17</b>	1.03
	No-Cosmetic	57.03	39.73	<b>17.16</b>	12.60	35.92	59.35	23.80	17.29	68.34	30.41	18.43	15.29
IITD Vista [33, 34]	No-No	99.75	-	2.27	-	99.75	-	2.35	-	100	-	<b>1.16</b>	-
	No-Soft	91.50	8.25	8.04	5.77	92.75	7.00	6.87	4.52	93.75	7.25	<b>5.31</b>	4.15
	No-Cosmetic	58.79	40.96	26.11	23.84	48.74	51.01	21.17	18.82	70.85	29.15	<b>12.62</b>	11.46
Our Dataset	No-No	99.79	-	3.34	-	99.69	-	3.81	-	99.89	-	<b>1.43</b>	-
	No-Soft	95.00	4.79	7.36	4.02	95.59	4.10	7.99	4.18	96.66	3.23	<b>4.86</b>	3.43
	No-Cosmetic	66.81	32.98	21.31	17.97	52.50	47.19	24.54	20.73	67.38	32.51	<b>19.59</b>	18.16
<b>Avg Degdn</b>	No-Soft	-	4.51	-	3.54	-	4.54	-	2.90	-	3.91	-	2.87
	No-Cosmetic	-	37.89	-	18.13	-	52.51	-	18.94	-	30.69	-	14.97

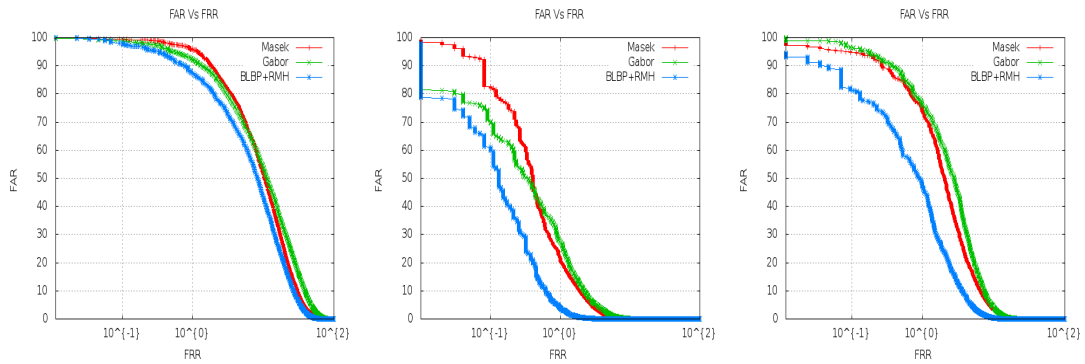
GC and PC stand for gallery class and probe class respectively. CRR and EER in %

Table 4.3: Performance Degradation due to use of Contact Lens

ROC curves shown in Figure 4.5 illustrates the comparison between iris recognition techniques. For each dataset, EER is minimum when recognition is carried out using BLBP+RMH approach except in the case when cosmetic lens images from IIITD Cogent dataset are matched with no lens images. Although BLBP+RMH performs the best among three techniques, none of these techniques can be said to perform sufficiently well for recognition purpose. Degradation in  $EER(D_{EER})$  and  $CRR(D_{CRR})$  represents the fall in recognition performance in the presence of lens. Average  $D_{EER}$  for three recognition techniques over all the datasets is 3.10% for soft lens and 17.32% for cosmetic lens while average  $D_{CRR}$  is 4.32% and 49.7% respectively.

ROC curves in Figure 4.6 supplement the results that cosmetic lens degrade the performance much more than soft lens. This can be attributed to the fact that soft lens is transparent in nature and unlike cosmetic lens, it does not have a pattern printed on its surface. However, partial reflection from the surface of soft lens creates artifacts in the iris region degrading the performance.

Figure 4.7 shows the genuine-impostor plots for the three datasets. The shift of genuine distribution towards impostor distribution for No-Soft and No-Cosmetic matchings conveys that genuine matchings are effected if soft lens or cosmetic lens is worn by a subject.

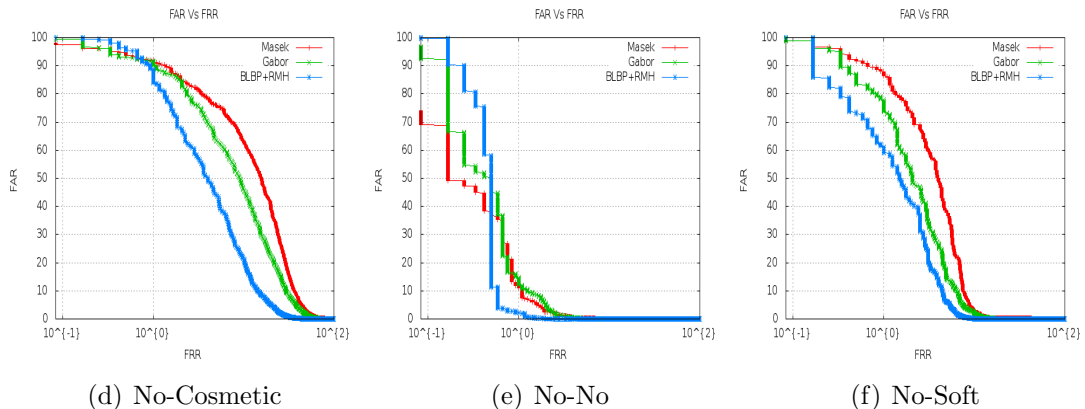


(a) No-Cosmetic

(b) No-No

(c) No-Soft

### Our Contact Lens dataset

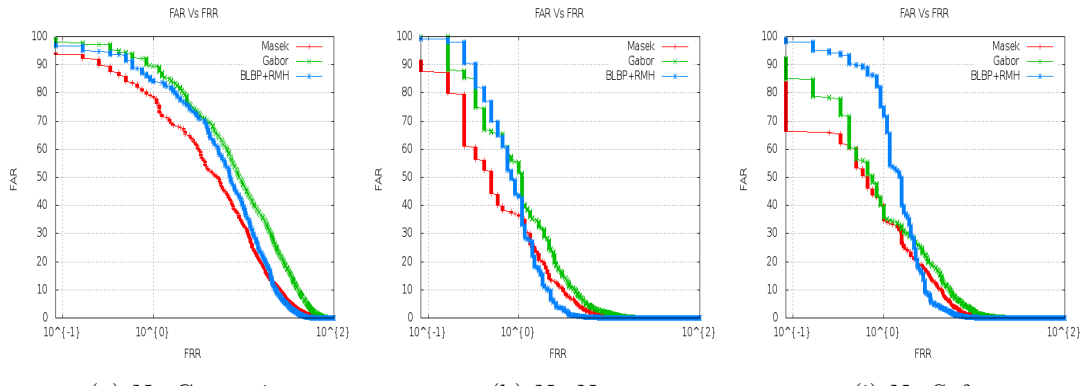


(d) No-Cosmetic

(e) No-No

(f) No-Soft

### IIITD Vista Contact Lens dataset



(g) No-Cosmetic

(h) No-No

(i) No-Soft

### IIITD Cogent Contact Lens dataset

**All the graphs use  $\log_{10}$  scale for X-axis**

Figure 4.5: Receiver Operating Characteristic(ROC) Curves

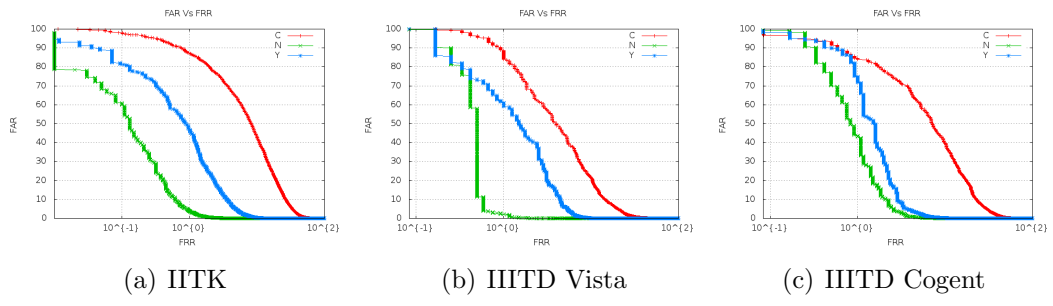


Figure 4.6: ROC Curve taking "No-Lens" Class as gallery Set

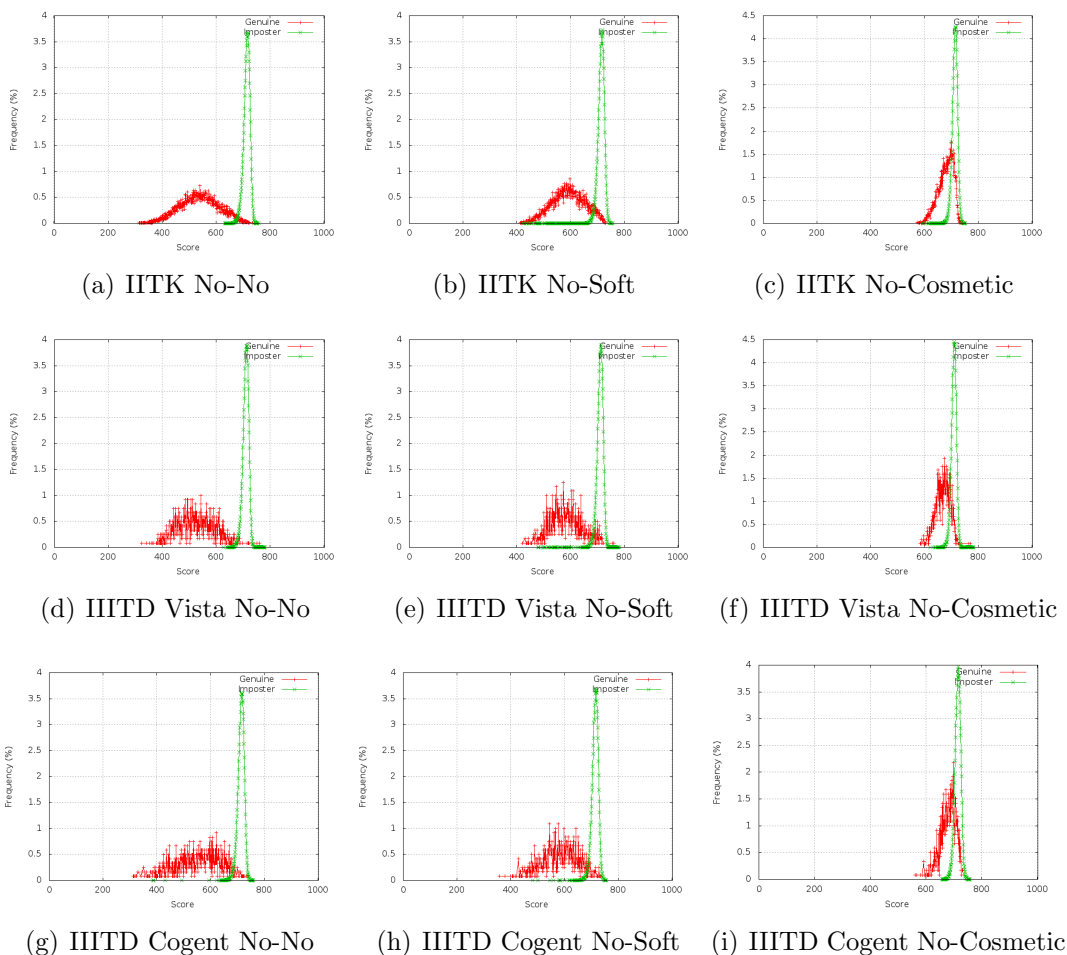


Figure 4.7: Genuine Imposter Plots

# Chapter 5

## Cosmetic Contact Lens Detection

This chapter proposes a cosmetic contact lens detection technique for iris biometric system. The acquired iris image has been segmented using the technique described in [37] and normalized using Daugman’s rubber sheet model. Fusion of texture based features LPQ and BGP have been used to construct feature vector for the normalized iris image. A pre-built classifier has been used to classify acquired iris images into cosmetic lens and without lens class. If the image is found to contain a cosmetic contact lens, subject is asked to remove the lens and re-enroll in the dataset.

### 5.1 Preprocessing

The acquired iris image has been thresholded to obtain a binary image. Morphological hole filling operations have been used to eliminate specular reflections from the iris image. Sobel filter has been used to detect edges on the binary image. Pupil, which is the darkest portion of iris , appears as a black portion at the center.

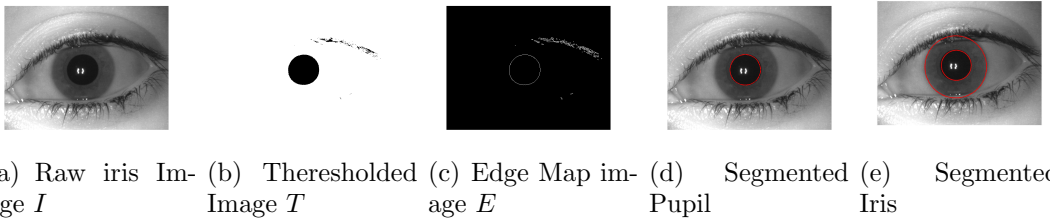


Figure 5.1: Iris Preprocessing

An improved version of Hough transform has been used to detect the boundary of pupil from the edge map [36, 38]. It makes the circle detection process faster by using the fact that center of the circle with edge point  $(x, y)$  lies along the direction normal to gradient  $\theta(x, y)$  at that point. The points lying at various distance in the direction of the gradient are potential candidates of pupil center.

Integro-differential operator has been applied over two non-occluded sectors of image. Taking the pupil center as a reference, every potential point in a window around it is assumed to be iris center. For every potential iris center, the contour where the intensity change is maximum as compared to previous contour is marked as iris boundary. This occurs because the surrounding limbic region has much higher intensity. To obtain normalized iris, the segmented iris image has been transformed from Cartesian to polar coordinates.

## 5.2 Cosmetic Lens Detection

As the textures of Cosmetic contact lenses differ from that of genuine iris, descriptors representing textures have been employed to generate feature vectors for their detection. The dataset has been split into training and test set. A supervised learning technique has been used to analyze instances of training data and infer

a function which has further been used to map training instances to their labels. Figure 5.2 describes the cosmetic lens detection process.

### 5.2.1 Training

66% of images from the dataset have been used for training the classifier. Each of the images have been assigned a label which conveys whether it belongs to cosmetic lens or no lens class. Images with subject wearing cosmetic contact lens have been assigned label +1 whereas the images in which subject is not wearing a lens have been assigned label -1. All images have been segmented and normalized. LPQ and BGP features have been extracted from the normalized images. 256-bin histogram obtained from LPQ and 216-bin histogram obtained from BGP features have been concatenated to form a 472-bit feature vector. Algorithm 1 and 2 describe the feature extraction process through LPQ and BGP features respectively. Scalar Vector Machine(SVM) has been used to learn the decision boundary between the two classes taking feature vector as attributes for each instance.

### 5.2.2 Prediction

33% of the dataset images have been used for testing the SVM model built in training step. The labels obtained from SVM have been compared to ground truth using performance matrices described in next section.

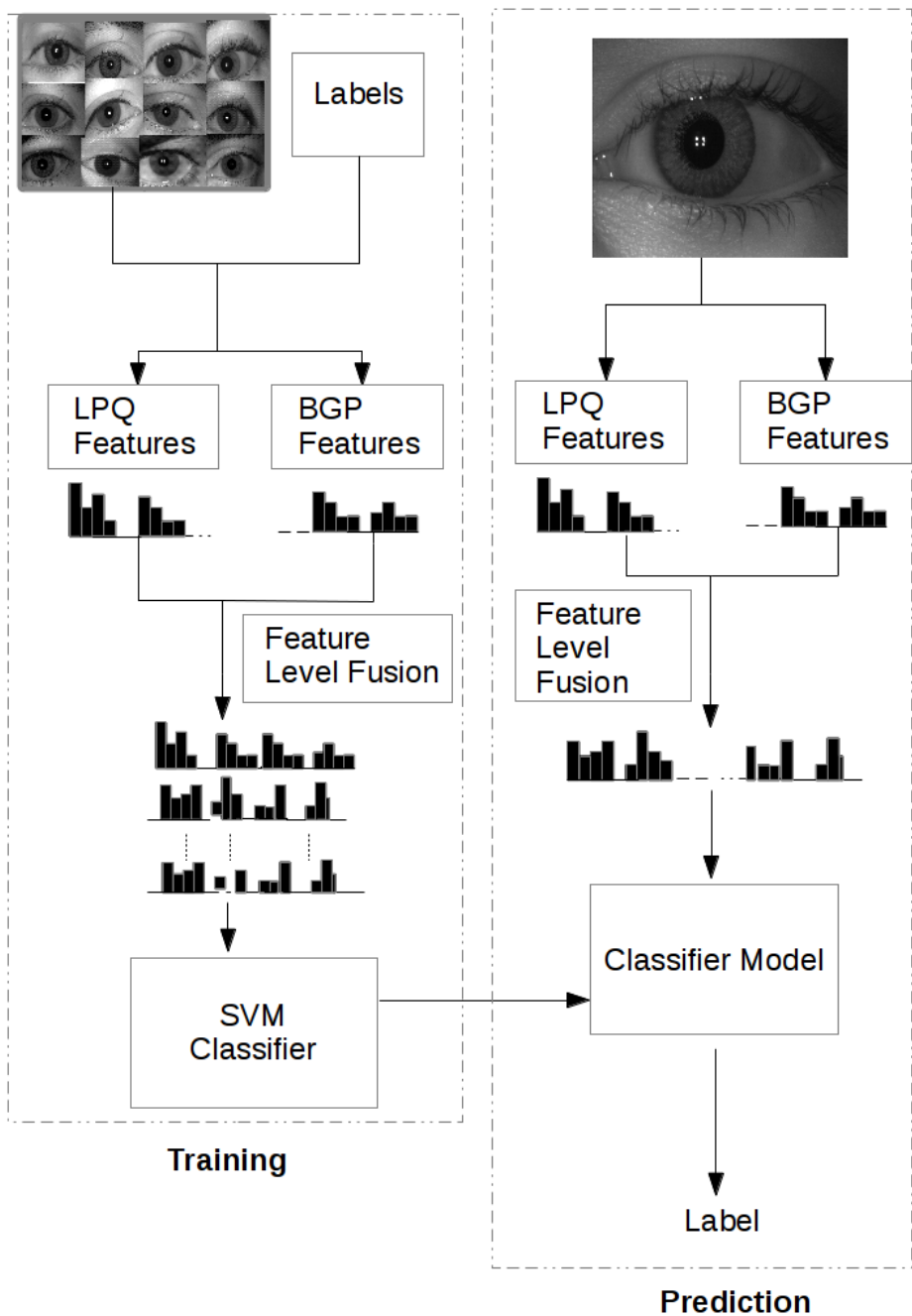


Figure 5.2: Lens Detection Process

---

**Algorithm 1** Local Phase Quantization Feature Extraction

---

**Require:**  $N$ : Normalized Iris of size  $h \times w$ ,  $W$ : window size for filter

**Ensure:**  $H$ : Histogram containing LPQ features

```
1: DFT_alpha= $\frac{1}{W}$  // the frequency for which DFT is calculated
2: N_d=DOUBLE(N)
3: halfLength= $\frac{W-1}{2}$  // radius of window size
4: x= -halfLength:halfLength// spatial coordinates of window
5: DFT_zero=x*0+1;
6: DFT_filter=EXP(COMPLEX(0,-2 *  $\pi$  * x * DFT_alpha)) // Creating 1D filters
7: DFT_filter_conj= CONJUGATE(DFT_filter)
8: filterResponse=CONV2(CONV2(N_d,DFT_zero),DFT_filter) // Compute fre-
   quency response
9: frequencyResponse=ZEROS(SIZE(filterResponse,1),SIZE(filterResponse,2),8)
10: frequencyResponse(:,:,1)=REAL(filterResponse)
11: frequencyResponse(:,:,2)=IMAG(filterResponse)
12: frequencyResponse=CONV2(CONV2(N_d,DFT_filter),DFT_zero)
13: frequencyResponse(:,:,3)=REAL(filterResponse)
14: frequencyResponse(:,:,4)=IMAG(filterResponse)
15: frequencyResponse=CONV2(CONV2(N_d,DFT_filter),DFT_filter)
16: frequencyResponse(:,:,5)=REAL(filterResponse)
17: frequencyResponse(:,:,6)=IMAG(filterResponse)
18: frequencyResponse=CONV2(CONV2(N_d,DFT_filter),DFT_filter_conjugate)
19: frequencyResponse(:,:,7)=REAL(filterResponse)
20: frequencyResponse(:,:,8)=IMAG(filterResponse)
21: [frequencyRow,frequencyColumns,frequencyNumber]=SIZE(frequencyResponse)
22: LPQHistogram=ZEROS(frequencyRow,frequencyColumns)
23: for i=1:frequencyNumber do
24:   LPQHistogram=LPQHistogram+DOUBLE(frequencyResponse(:,:,i)>0)*( $2^{i-1}$ )
25: end for
26: LPQHistogram=LPQHistogram/sum(LPQHistogram)
27: return (LPQHistogram)
```

---

### 5.3 Lens Detection Results

Apart from the three datasets described in Section 4.1 , an additional dataset UND is also used for detection of contact lens.

UND Contact lens dataset contains iris images acquired in a windowless acquisition room. There are three lens classes [‘C’, ‘N’, ‘Y’] corresponding to contact lens, no lens and soft lens respectively. Table 5.1 summarizes the this dataset. Some of the sample images from the dataset are shown in Figure 5.3.

<b>Types of Contact Lens</b>	Cosmetic lens,Soft lens and no lens
<b>Cosmetic Lens Manufacturers</b>	CibaVision,Johnson & Johnson,CooperVision
<b>Cosmetic Lens Color</b>	Honey,Green,Blue,Gray
<b>Iris Sensor</b>	LG 4000
<b>Images per class</b>	C:1400,N:1400,Y:1400
<b>Minimum images per eye class</b>	5
<b>Total Images</b>	4200

Table 5.1: UND Contact Lens Dataset Summary



Figure 5.3: Sample Images from UND Contact Lens dataset

### 5.3.1 Performance Metrics

The labels obtained from classification have been compared to ground truth labels. Our approach has been compared to earlier approaches through two performance metrics - Correct Classification Rate (CCR) and False Acceptance Rate (FAR).

### 5.3.1.1 CCR

Correct classification rate gives the percentage of test images that have been correctly classified by the model. It has been represented by :-

$$FRR(t) = \frac{TP + TN}{TP + TN + FP + FN} \times 100 \quad (5.1)$$

where  $TP$ ,  $TN$ ,  $FP$  and  $FN$  are True Positives, True Negatives, False Positives and False Negatives respectively.

### 5.3.1.2 FAR

False Acceptance Rate denotes the number of images having cosmetic lens misclassified as without lens. FAR is an important metric for cosmetic lens detection as it quantifies the probability of a criminal evading detection by using a cosmetic contact lens. It is given by :-

$$FRR(t) = \frac{FP}{TN + FP} \times 100 \quad (5.2)$$

## 5.3.2 Experimental Results

Our approach has been compared with GLCM [39],LBP [20] adn BSIF [21] approach. For GLCM, we have used the mean of inverse difference moment ( $f_{idm}$ ), sum average ( $f_{sa}$ ) and sum entropy ( $f_{sum}$ ) as features as mentioned in [39]. For LBP, we have concatenated histograms of two operators  $LBP_{8,1}^{riu2}$  and  $LBP_{16,2}^{riu2}$  to form a feature vector. The radius and size of features learnt in BSIF are taken to be 3 and 12 respectively as these parameters had provided consistant results in

[21]. In our own approach, BGP features extracted at three resolutions ( $\lambda_i, \sigma_i$ ) set as (1.3,0.7),(5.2,2.5) and (22,4.5) have been concatenated to form feature vector.

Scalar Vector Machine (SVM) with radial basis kernel has been used for classification purpose. The correct classification rate and False Acceptance Rate for different lens detection techniques is shown in Table 5.2. For IIITD Vista, IIITD Cogent and UND datasets, the technique clearly outperforms all other cosmetic lens detection techniques in terms of FAR. BSIF slightly outperforms the method over IITK dataset due to its generalizing property as it contains four varieties of cosmetic contact lens.

Descriptor	GLCM[39]		LBP[20]		BSIF[21]		LPQ+BGP	
Dataset	CCR	FAR	CCR	FAR	CCR	FAR	CCR	FAR
Our dataset	57.05	30.02	97.54	0.55	98.44	<b>0.55</b>	<b>98.91</b>	0.86
IIITD Vista	50.00	55.88	99.70	0.58	99.70	0.58	<b>99.85</b>	<b>0.29</b>
IIITD Cogent	36.86	46.07	89.54	12.91	<b>98.21</b>	3.29	96.81	<b>2.82</b>
UND	56.59	31.11	95.82	6.22	85.93	28.44	<b>99.12</b>	<b>1.55</b>

Table 5.2: CCR and FAR across Various Texture Description Techniques

---

**Algorithm 2** Binary Gabor Pattern Feature Extraction

---

**Require:**  $N$ : Normalized Iris of size  $h \times w$

**Ensure:**  $H$ : Histogram containing BGP features

```
1: N_d = DOUBLE(N) // Converting uint8 to double
2: N_mean = MEAN(N_d)
3: N_std = STD(N_d) // Standard deviation of image matrix
4: N = (N - N_mean)./N_std // Remove the DC component of image
5: numOrientations = 8 // Number of Orientations for Gabor filters
6: G = gaborArray(h,w) // creates a gabor filter bank for a given wavelength,scale
   and aspect ratio,
7: halfLength=17 // Radius of the patch to be used
8: filterRows=2*halfLength+1
9: filterColumns=2*halfLength+1
10: fftRows=h+filterRows-1
11: fftColumn=w+filterColumn-1 // Setting the size of FFT
12: N_fft=FFT2(N,fftrows,fftColumns)
13: H =ZEROS(216,1) // Initializing the Histogram with zeros
14: evenGaborResponse=ZEROS(h-2*halfLength,w-2*halfLength,8) // To cap-
   ture real part of Gabor response
15: oddGaborResponse = ZEROS( h-2*halfLength,w-2*halfLength,8) // To cap-
   ture imaginary part of Gabor response
16: scale=[(0.7,1.3) (2.5,5.2) (4.5,22)] // set of values for wavelength and scale of
   Gabor filter bank
17: for scaleIndex=1 to 3 in steps of 1 do
18:   evenHistScale=ZEROS(36,1) // Initialize scale level histogram with zeros
19:   oddHistScale=ZEROS(36,1)
20:   for orientationIndex=1 to numOrientations in steps of 1 do
21:     gaborResponse =IFFT2( N_fft .* gabor(:,:,orientationIndex)) // Inverse
       Fourier transform
22:     evenGaborResponse(:,:,orientationIndex)=real(gaborResponse(2*halfLength+1:h,
      2*halfLength+1:w))
23:     oddGaborResponse(:,:,orientationIndex)=imaginary(gaborResponse(2*halfLength+1:h,
      2*halfLength+1:w))
24:   end for
25:   evenBinaryResponse=evenGaborResponse > 0
26:   oddBinaryResponse=oddGaborResponse > 0
27:   evenHist=ZEROS(h-2*halfLength,w-2*halfLength)
28:   oddHist=ZEROS(h-2*halfLength,w-2*halfLength)
```

---

---

```
29: for orientationIndex=1 to numOrientations in steps of 1 do
30:   evenHist=evenHist+evenBinaryResponse(:,:,orientationIndex)*2orientationIndex-1
31:   oddHist=oddHist+oddBinaryResponse(:,:,orientationIndex)*2orientationIndex-1
32: end for
33: evenHistNormalized=evenHist/SUM(evenHist)
34: oddHistNormalized=oddHist/SUM(oddHist)
35: H((scaleIndex-1)*72+1,(scaleIndex-1)*72+36)=evenHistNormalized
36: H((scaleIndex-1)*72+37,scaleIndex*72 )=oddHistNormalized
37: end for
38: return (H)
```

---

# Chapter 6

## Conclusions and Future Work

### 6.1 Conclusions

This thesis has evaluated the effects of contact lenses on iris recognition. A dataset has been introduced which contains images of 100 eye classes corresponding to cosmetic lens, soft lens and no lens class. It is found to be the largest contact lens dataset in terms of number of acquired images. Average degradation in EER for three recognition techniques over all datasets is 3.10% for soft lens and 17.32% for cosmetic lens while average degradation in CRR is 4.32% and 49.7% respectively. These results have firmly established the degradation in recognition performance both in the case of soft and cosmetic contact lens. However, the degradation is much more when a subject is wearing a cosmetic contact lens in comparison pattern printed on it occludes most of the iris texture.

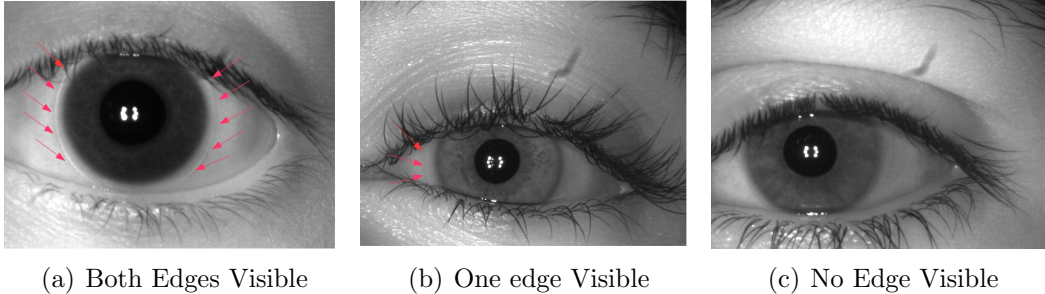
Further, an approach has been proposed for detecting cosmetic contact lens at the time of image acquisition. The acquired image is first segmented and normalized. LPQ and BGP features are extracted and concatenated to form a feature

vector for the image. A pre-built SVM model is used to classify the image into cosmetic lens or no lens class. Existing cosmetic lens detection techniques are compared with the proposed technique that uses fusion of LPQ and BGP texture descriptors. The proposed technique has outperformed LBP, GLCM and BSIF based techniques for IIITD Vista, IIITD Cogent and UND datasets. BSIF performed slightly better than our technique over IITK dataset as there were four different cosmetic lens classes present in the dataset. However, our approach performs significantly better than BSIF for UND dataset which contains blurred images.

The proposed lens detection approach can be plugged into any existing iris recognition system to know if a user is wearing a cosmetic contact lens at the time of image acquisition. This would prevent malicious subjects from voluntarily spoofing the system and gaining illegitimate access to privileges.

## 6.2 Future Work

An approach needs to be devised for detecting soft contact lens. As shown in Table 4.3, presence of soft contact lens degrades both the verification and identification performance. Due to varying illumination, the edges of soft contact lens are not even visible to human eye in some of the images. The only work addressing the detection of soft contact lens is in [3] with a CCR of 76% and 66.5% on ICE 2005 and MBGC dataset respectively. Figure 6.1 contains some of the example images from IITK contact lens dataset showing the variation in discernibility of soft lens. Image 6.1(c) shows an eye containing soft contact lens with insignificant boundary. It is also not reasonable to assume prior knowledge about the sensors



(a) Both Edges Visible      (b) One edge Visible      (c) No Edge Visible

Figure 6.1: Example Images with Soft Lens in IITK Dataset

and different cosmetic lens patterns. Thus, a need of generalized texture detection algorithm arises which can operate under varying conditions. This would involve creating an ensemble of various lens-specific techniques or designing a new feature representation. Other possible area is to explore whether the cosmetic contact lens



(a) All White      (b) All Black      (c) Hallowen Style

Figure 6.2: Unconventional Lenses Available in the Market [3]

detection problem be better formulated as a one class problem rather than two class classification as proposed in the thesis. If it could be formulated as a single class classification problem, it would be sufficient to learn the texture of genuine iris rather than training on textural features of various cosmetic lenses. Some unconventional cosmetic lenses are shown in Figure 6.2 which could be successfully detected through this approach.

# Bibliography

- [1] Vista Imaging Incorporated. [http://www.vistaimaging.com/FA2\\_product.html](http://www.vistaimaging.com/FA2_product.html). Accessed: 2014-10-11.
- [2] Juho Kannala and Esa Rahtu. Bsif: Binarized statistical image features. In *21st International Conference on Pattern Recognition (ICPR)*, pages 1363–1366. IEEE, 2012.
- [3] Eyesbright Inc. <http://www.eyesbright.com>. Accessed: 2014-11-05.
- [4] Leonard Flom and Aran Safir. Iris recognition system, February 3 1987. US Patent 4,641,349.
- [5] John Daugman. How iris recognition works. In *Proceedings of International Conference on Image Processing (ICIP 2002)*, pages 33–36, 2002.
- [6] John Daugman. New methods in iris recognition. *IEEE Transactions on Systems, Man, and Cybernetics, Part B: Cybernetics*, 37(5):1167–1175, 2007.
- [7] J.R. Matey, O. Naroditsky, K. Hanna, R. Kolczynski, D.J. LoIacono, S. Mangru, M. Tinker, T.M. Zappia, and W.-Y. Zhao. Iris on the move: Acquisition of images for iris recognition in less constrained environments. *Proceedings of the IEEE*, 94(11):1936–1947, 2006.

- [8] Faisal Bashir, Pablo Casaverde, David Usher, and Marc Friedman. Eagle-eyes: a system for iris recognition at a distance. In *Proceedings of IEEE Technologies for Homeland Security Conference on*, pages 426–431. IEEE, 2008.
- [9] Dae Sik Jeong, Hyun-Ae Park, Kang Ryoung Park, and Jaihie Kim. Iris recognition in mobile phone based on adaptive gabor filter. In *Advances in Biometrics*, pages 457–463. Springer, 2005.
- [10] Nathan D Kalka, Jinyu Zuo, Natalia A Schmid, and Bojan Cukic. Image quality assessment for iris biometric. In *Defense and Security Symposium*, pages 62020D–62020D. International Society for Optics and Photonics, 2006.
- [11] R.P. Wildes. Iris recognition: an emerging biometric technology. *Proceedings of the IEEE*, 85(9):1348–1363, 1997.
- [12] Y.P. Huang, S.W. Luo, and E.Y. Chen. An efficient iris recognition system. In *Proceedings of the International Conference on Machine Learning and Cybernetics*, volume 1, pages 450–454. IEEE, 2002.
- [13] Zhaofeng He, Tieniu Tan, Zhenan Sun, and Xianchao Qiu. Toward accurate and fast iris segmentation for iris biometrics. *IEEE Transactions on Pattern Analysis and Machine Intelligence*, 31(9):1670–1684, 2009.
- [14] Roger A Freedman and Hugh D Young. *University Physics*. Addison-Wesley, 2008.
- [15] Zhaofeng He, Tieniu Tan, Zhenan Sun, and Xianchao Qiu. Robust eyelid, eyelash and shadow localization for iris recognition. In *Proceedings of 15th*

*IEEE International Conference on Image Processing*, pages 265–268. IEEE, 2008.

- [16] A.K. Bachoo and J.R. Tapamo. Texture detection for segmentation of iris images. In *Proceedings of the 2005 Annual Research Conference of the South African Institute of Computer Scientists and Information Technologists on IT Research in Developing Countries*, pages 236–243, 2005.
- [17] Eui Chul Lee, Kang Ryoung Park, and Jaihie Kim. Fake iris detection by using purkinje image. In *Advances in Biometrics*, pages 397–403. Springer, 2005.
- [18] Ken Hughes and Kevin W Bowyer. Detection of contact-lens-based iris biometric spoofs using stereo imaging. In *46th Hawaii International Conference on System Sciences (HICSS)*, pages 1763–1772. IEEE, 2013.
- [19] John Daugman. Demodulation by complex-valued wavelets for stochastic pattern recognition. *International Journal of Wavelets, Multiresolution and Information Processing*, 1(01):1–17, 2003.
- [20] Zhaofeng He, Zhenan Sun, Tieniu Tan, and Zhuoshi Wei. Efficient iris spoof detection via boosted local binary patterns. In *Advances in Biometrics*, pages 1080–1090. Springer, 2009.
- [21] Hadid A Pietikinen M Komulainen J. Generalized textured contact lens detection by extracting bsif description from cartesian iris images. Proceedings of International Joint Conference on Biometrics (IJCB 2014), Clearwater, FL.

- [22] Zhenan Sun, Hui Zhang, Tieniu Tan, and Jianyu Wang. Iris image classification based on hierarchical visual codebook. *IEEE Transactions on Pattern Analysis and Machine Intelligence*, 2014.
- [23] L. Masek et al. Recognition of human iris patterns for biometric identification. *M.Tech Thesis, The University of Western Australia*, 2003.
- [24] D.M. Monro, S. Rakshit, and D. Zhang. Dct-based iris recognition. *IEEE Transactions on Pattern Analysis and Machine Intelligence*, 29(4):586–595, 2007.
- [25] Zhenan Sun, Tieniu Tan, and Xianchao Qiu. Graph matching iris image blocks with local binary pattern. In *Proceedings of the 2006 international conference on Advances in Biometrics*, pages 366–372, 2006.
- [26] Maria De Marsico, Michele Nappi, and Daniel Riccio. Noisy iris recognition integrated scheme. *Pattern Recognition Letters*, 33(8):1006–1011, 2012.
- [27] Aditya Nigam, Vamshi Krishna G, and Phalguni Gupta. Iris recognition using block local binary patterns and relational measures. In *Proceeding of International Joint Conference on Biometrics*, pages 1–7. IEEE, 2014.
- [28] J.G. Daugman. High confidence visual recognition of persons by a test of statistical independence. *IEEE Transactions on Pattern Analysis and Machine Intelligence*, 15(11):1148–1161, 1993.
- [29] Robert M Haralick, Karthikeyan Shanmugam, and Its' Hak Dinstein. Textural features for image classification. *IEEE Transactions on Systems, Man and Cybernetics*, (6):610–621, 1973.

- [30] Timo Ojala, Matti Pietikäinen, and Topi Mäenpää. Multiresolution gray-scale and rotation invariant texture classification with local binary patterns. *IEEE Transactions on Pattern Analysis and Machine Intelligence.*, 24(7):971–987, 2002.
  - [31] Mark R Banham and Aggelos K Katsaggelos. Digital image restoration. *IEEE Signal Processing Magazine*, 14(2):24–41, 1997.
  - [32] Richard W Hamming. Error detecting and error correcting codes. *Bell System Technical Journal*, 29(2):147–160, 1950.
  - [33] Daksha Yadav, Naman Kohli, JS Doyle, Richa Singh, Mayank Vatsa, and Kevin W Bowyer. Unraveling the effect of textured contact lenses on iris recognition. *IEEE Transactions on Information Forensics and Security*, 2014.
  - [34] Naman Kohli, Daksha Yadav, Mayank Vatsa, and Richa Singh. Revisiting iris recognition with color cosmetic contact lenses. In *Proceedings of International Conference on Biometrics (ICB)*, pages 1–7. IEEE, 2013.
  - [35] Kevin W Bowyer, Karen Hollingsworth, and Patrick J Flynn. Image understanding for iris biometrics: A survey. *Computer vision and image understanding*, 110(2):281–307, 2008.
  - [36] Amit Bendale, Aditya Nigam, Surya Prakash, and Phalguni Gupta. Iris segmentation using improved hough transform. In *Emerging Intelligent Computing Technology and Applications*, volume 304 of *Communications in Computer and Information Science*, pages 408–415. Springer Berlin Heidelberg, 2012.

- [37] Amit Bendale, Aditya Nigam, Surya Prakash, and Phalguni Gupta. Iris segmentation using improved hough transform. In *Emerging Intelligent Computing Technology and Applications*, pages 408–415. Springer, 2012.
- [38] Aditya Nigam and Phalguni Gupta. Iris recognition using consistent corner optical flow. In *Proceedings of the 11th Asian conference on Computer Vision*, pages 358–369, 2013.
- [39] Zhuoshi Wei, Xianchao Qiu, Zhenan Sun, and Tieniu Tan. Counterfeit iris detection based on texture analysis. In *Proc. 19th International Conference on Pattern Recognition*, pages 1–4. IEEE, 2008.